Two-Dimensional Pulsed Propagation From Extended Planar Aperture Field Distributions Through a Planar Dielectric Layer via Quasi-Ray Gaussian Beams

Vincenzo Galdi, *Member, IEEE,* and Leopold B. Felsen, *Life Fellow, IEEE*

***Abstract*—A previously developed Gabor-based quasiray *narrow-waisted* (NW) Gaussian beam (GB) algorithm for time-harmonic propagation of aperture-excited two-dimensional (2-D) electromagnetic fields through a planar dielectric layer (Maciel and Felsen) is extended here to the time domain (TD) to deal with short-pulse excitation. The dielectric layer is assumed to be nondispersive; however, slight Ohmic losses can be accommodated. The frequency domain (FD) algorithm is based on a self-consistent discretization of the aperture field distribution in terms of basis NW-GBs in conjunction with an efficient *quasireal* ray tracing scheme for tracking the individual basis beams. The TD results are obtained by analytic Fourier inversion from the FD in terms of pulsed beam wavepackets, following a procedure similar to that utilized in (Galdi *et al.*) in connection with free-space aperture radiation. The proposed algorithm is validated and calibrated against a rigorous numerical reference solution via an extensive series of numerical experiments. *A priori* accuracy assessments in terms of critical nondimensional estimators, and computational costs, are also given attention.**

***Index Terms*—Gaussian beam wavepackets, layered media, short pulses.**

I. Introduction

PROPAGATION of electromagnetic (EM) wavefields in the presence of layered dielectric media is a problem of long-standing interest. For canonical coordinate-separable geometries (i.e., planar, circular cylindrical, spherical), *spectral wavenumber techniques* constitute the natural choice for rigorous analytic investigation, primarily in the frequency domain (FD), but also in the time domain (TD) (see, e.g., [3]–[7]). However, in the presence of *arbitrarily* shaped layered structures, exact analytic techniques are no longer applicable, and one is led to employ either approximate semi-analytic approaches or brute-force numerical algorithms. In this connection, for aperture-excited configurations in the asymptotic high-frequency limit, Gabor-based *narrow-waisted* (NW) Gaussian beam (GB) algorithms have been shown to provide a versatile and robust approximate tool which, though preserving the attractive computational features of standard ray-optical techniques, does *not* fail in typical ray-field transition regions. The NW-GB decomposition on the Gabor lattice discretizes the aperture field distribution and permits efficient *quasireal complex ray tracing* (via the *complex source point* (CSP) method) of individual basis beams through the environment, with eventual recombination to synthesize the total field at the observer [8]. In the FD, this approach has been applied successfully to propagation through arbitrarily shaped dielectric layers, for both two-dimensional (2-D) fields radiated by 1-D aperture distributions [1], [9], and 3-D fields radiated by 2-D aperture distributions [10]. Accurate predictions over calibrated parameter ranges have been obtained with modest computational effort.

The results in [1], [8]–[10] can be extended formally to *pulsed* excitations via inversion from the FD to the TD. However, for the ultra-wideband pulsed excitations of practical interest in modern communication systems, it is suggestive to explore a formulation in terms of *pulsed beam* (PB) wavepackets, which is better matched to the short-pulse wave phenomenology and can therefore be expected to yield better numerical efficiency as well as deeper physical insight. These considerations have motivated our recent stepwise extensions of the FD NW-GB algorithms in [1], [8]–[10] to the TD, starting with the free-space pulsed propagation from extended 1-D [2] and 2-D [11] aperture field distributions, and subsequently including TD reflection from, and transmission through, moderately rough dielectric interfaces [12], [13] (although the logical canonical escalation for a single dielectric interface involves a *planar* profile, we diverted to the asymptotically approximated fields in the presence of the rough profile because of our simultaneous interest in buried object identification). In the present paper, we return *directly* to the plane stratified canonical configuration in [1] which treats FD 2-D fields excited by 1-D aperture distributions in the presence of a planar dielectric layer, but now excited by a TD 1-D truncated tapered aperture field distribution. Proceeding as in [2], the FD NW-GB synthesis for the transmitted field obtained in [1] is inverted analytically to the TD, yielding a *closed form* representation in terms of rapidly computable confluent hypergeometric functions. As in [2], propagation-matched *tilted* PBs are used for more effective modeling of possible linear phasing (delay) in the aperture field distribution. The dielectric layer is assumed to be nondispersive; however,

Manuscript received March 18, 2002; revised July 23, 2002. This work was supported in part by a European Union postdoctoral fellowship through the University of Sannio, Benevento, Italy, the U.S.-Israel Binational Science Foundation under Grant 9900448, and the Polytechnic University, Brooklyn, NY.

V. Galdi was with the Department of Electrical and Computer Engineering, Boston University, Boston, MA 02215 USA, and is now with the Department of Engineering, University of Sannio, Benevento, Italy (e-mail: vgaldi@unisannio.it).

L. B. Felsen is with the Department of Aerospace and Mechanical Engineering and the Department of Electrical and Computer Engineering, Boston University, Boston, MA 02215 USA, and also with Polytechnic University, Brooklyn, NY 11201 USA (e-mail: lfelsen@bu.edu).

Digital Object Identifier 10.1109/TAP.2003.813629

slight Ohmic losses can be accommodated via an appropriate *nondispersive* approximation.

The layout of the paper is as follows. In Section II, the problem is formulated, with definition of the notation used throughout the paper. In Section III, the FD formulation in [1] is briefly reviewed, and is modified slightly in order to facilitate its subsequent analytic inversion to the TD. Section IV deals with the TD inversion, along the guidelines pursued in [2]. Simplifying approximations are utilized and accuracy assessments are quantified analytically in terms of critical nondimensional estimators. In the synthetic numerical experiments of Section V, the above solution strategy is validated and calibrated against an independently generated numerical reference solution obtained via brute-force integration of the rigorous plane-wave spectral integrals. Typical examples selected from a broad range of numerical simulations of the layer-transmitted fields excited by linearly and nonlinearly phased (e.g., focusing) TD aperture distributions are presented and discussed for various combinations of the problem parameters, with emphasis on accuracy and computational issues. Conclusions follow in Section VI.

II. Statement of the Problem

The problem geometry is illustrated in Fig. 1. In a 2-D (x,z) reference system, an EM transient field with transverse magnetic (TM) polarization impinges on an infinite plane dielectric layer with lower interface at $z=z_L$, thickness d_1, relative permittivity ϵ_{r1}, and electrical conductivity σ_1. The time domain (TD) incident field e_y^i is generated by a 1-D truncated planar pulsed y-directed aperture field distribution which occupies the region $|x|\le d/2$ at $z=0$ where the space-time distribution of the incident tangential electric field is specified

$$e_y^i(x,z=0,t)=\begin{cases} f(x,t), & |x|\le \frac{d}{2},\\ 0, & |x|>\frac{d}{2}. \end{cases} \tag{1}$$

Lower case letters denote TD fields. In what follows, we restrict our attention to slightly lossy layers, i.e., $\sigma_1/\omega\epsilon_0\epsilon_{r1}\ll 1$, with ω being the angular frequency. Both ϵ_{r1} and σ_1 are assumed to be frequency independent. As in [2], we use tapered aperture field distributions with separable space-time dependence and general nonlinear time delay

$$f(x,t)=g(x)p\left[t-c_0^{-1}\phi(x)\right] \tag{2}$$

where $g(x)$ is a spatial tapering function which vanishes at $x=\pm d/2$, $c_0=(\epsilon_0\mu_0)^{-1/2}$ is the free-space wavespeed, $p(t)$ is a time pulse with characteristic duration $T\ll d/c_0$, and $\phi(x)$ is a general nonlinear phase (delay) function. Recalling the efficient treatment of linear delay fields [2, Sec. II-C], it is convenient to split $\phi(x)$ into a linear part plus a nonlinear remainder

$$\phi(x)=x\sin\theta_A+\phi_{NL}(x) \tag{3}$$

where θ_A is a real angle, and $\phi_{NL}(x)$ does not contain linear terms.

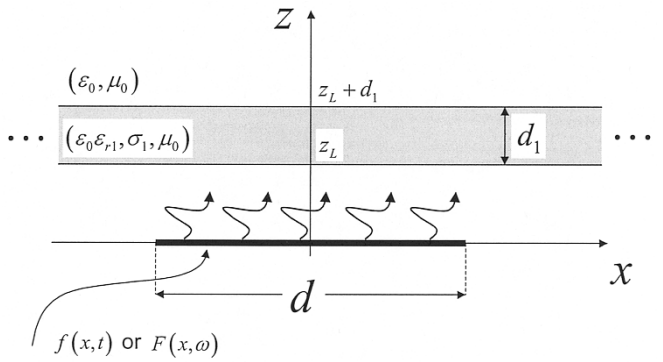

Fig. 1. Problem geometry: a large truncated aperture field distribution of width d, with space-time dependence $f(x,t)$ and temporal spectrum $F(x,\omega)$, radiates in the presence of a homogeneous dielectric layer of thickness d_1, with relative dielectric permittivity ϵ_{r1} and electrical conductivity σ_1. The field is observed in the half-space $z>z_L+d_1$. The numerical simulations in Section V results have been carried out for $z_L=0$.

In computing the space-time EM field transmitted through the dielectric layer into the halfspace $z>z_L+d_1$, we restrict our attention to the y-directed electric field $e_y^t(x,z,t)$ from which all other field quantities of interest can be obtained via Maxwell's equations. Note that, for this geometry, the layer-transmitted field does not depend on the layer location z_L between the aperture and the observation plane (see [1] and Section III-A-2). Throughout the paper, the TD is accessed by inversion from the FD via the temporal Fourier transform pair

$$\begin{aligned} f(t)&=\frac{1}{2\pi}\int_{-\infty}^{\infty}F(\omega)\exp(-i\omega t)d\omega,\\ F(\omega)&=\int_{-\infty}^{\infty}f(t)\exp(i\omega t)dt \end{aligned} \tag{4}$$

with FD quantities identified by capital letters. However, we shall also use the positive frequency analytic transform [14], when convenient

$$\begin{aligned} \overset{+}{f}(t)&=\frac{1}{\pi}\int_{0}^{\infty}F(\omega)\exp(-i\omega t)d\omega,\quad \mathrm{Im}(t)\le 0,\\ f(t)&=\mathrm{Re}\left[\overset{+}{f}(t)\right]. \end{aligned} \tag{5}$$

Frequent reference will be made to results in [1], [2], and [12], with $(\alpha.\beta)$ denoting equation (β) in reference $[\alpha]$; for instance, (2.4) means (4) in [2].

III. Frequency Domain (FD) Formulation

This section contains a brief summary of relevant frequency domain (FD) results from [1], [2] and some new additions. The FD aperture field corresponding to (2) has an implicit $\exp(-i\omega t)$ time dependence and a spatial distribution $F(x,\omega)$

[related to $f(x,t)$ via the Fourier transform pair in (4)] over the aperture in Fig. 1

$$F(x,\omega) = g(x)P(\omega)\exp\left[ik_0\phi(x)\right] \tag{6}$$

where $k_0 = \omega/c_0 = 2\pi/\lambda_0$ is the free-space wavenumber, with λ_0 denoting the free-space wavelength, and $P(\omega)$ represents the FD spectrum of the pulse $p(t)$. In the remainder of this section, the ω dependence will be omitted for simplicity of notation.

A. Gabor-Based Narrow-Waisted Gaussian Beam (NW-GB) Discretization

1) NW-GB Synthesis of FD Radiated Field in Free Space: Following [2, Sec. II-C], the FD field radiated into free space by the aperture field distribution in (6) can be parameterized in terms of *propagation-matched* tilted NW-GBs as

$$E_y^i(x,z) \approx \sum_{|m|\leq\left(\frac{d}{2L_x}\right)} A_m \tilde{\mathcal{B}}_m(x,z) \tag{7}$$

where the amplitude coefficients A_m can be estimated efficiently by sampling the aperture profile at the Gabor lattice points $x_m = mL_x$ [cf. (2.19)]

$$\begin{aligned} A_m &= \left(\frac{L_x}{\sqrt{2}}\right)^{\frac{1}{2}} F(x_m)\exp(-ik_0 x_m \sin\theta_A) \\ &= \left(\frac{L_x}{\sqrt{2}}\right)^{\frac{1}{2}} g(x_m)P(\omega)\exp\left[ik_0\phi_{NL}(x_m)\right], \\ &\quad |m| \leq \left(\frac{d}{2L_x}\right) \end{aligned} \tag{8}$$

with L_x denoting the lattice period (for NW-GBs, $L_x \lesssim \lambda_0 \ll d$), and ϕ_{NL} being defined in (3). The NW-GB propagators $\tilde{\mathcal{B}}_m$ in (7) can be approximated efficiently via complex-source-point (CSP) asymptotics, and their expression is given in (2.20). The reader is referred to [2] for the analytical (constraint) and computational implications of these approximations. In (7) and henceforth, the tilde˜identifies dependence on analytically continued spatial source coordinates as well as the field produced thereby.

2) NW-GB Synthesis of Layer-Transmitted Field: The GB-discretized radiated aperture field transmitted through the layer is computed by tracking the NW-GB basis functions $\tilde{\mathcal{B}}_m$ in (7) *individually*, and eventually recombining them at the observer. As shown in [1], implementation of the rigorous complex ray machinery [15], [16] for NW-CSP GBs can be simplified substantially by computationally efficient *quasireal* ray tracing schemes that involve paraxial beam shooting. In [1, Sec. II-B], this procedure has been used for tracking a multi-hop GB along its real-ray axis via conventional real ray tracing; the slightly complex NW-GB spectrum of the emerging GB is accounted for approximately through augmentation of its on-axis (real ray) value by a complex phase correction in the distance from the axis to the off-axis observer. Here, we use a slightly different, though similarly motivated approximation as noted below. The *total* transmitted field due to the GB-discretized incident field in (7) is given by [cf. (1.19)]

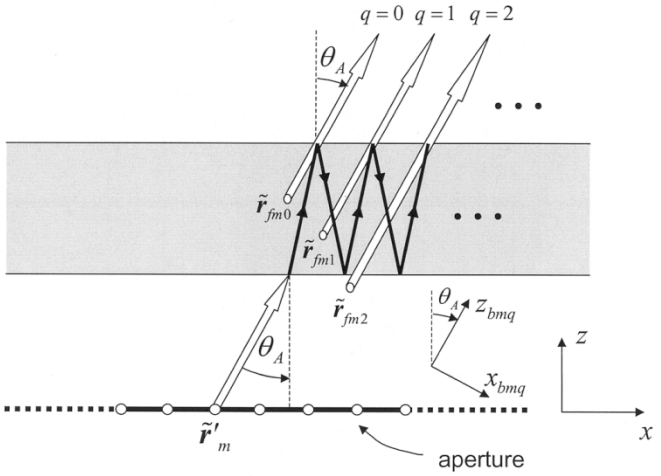

Fig. 2. Schematic interpretation of the *quasireal* ray-tracing scheme pertaining to transmission of a single NW-CSP beam through the layer [cf. (9) and (11)]. A *complex ray* is traced from the CSP at $\bar{\mathbf{r}}'_m$ along a *complex* trajectory to the intersection of the *real* beam axis with the *real* layer (lower) interface; the path into the layer proceeds entirely in *real* space along the beam axis, undergoing q round-trip reflections inside the dielectric layer. The last segment, which reaches the observer, proceeds in *complex* space as a *complex ray* emanating from the complex virtual focus $\bar{\mathbf{r}}_{fmq}$. In real configuration space, these complex rays describe NW paraxial Gaussian beams. White arrows denote complex rays; black arrows denote real rays; "∘" denotes the locations of the complex source points $\bar{\mathbf{r}}'_m \equiv (x_m + ib\sin\theta_A, ib\cos\theta_A)$ and the complex virtual foci $\bar{\mathbf{r}}_{fmq} \equiv (\bar{x}_{fmq}, \bar{z}_{fq})$ in (14) and (15). The beam coordinates (x_{bmq}, z_{bmq}) are sketched in the inset.

$$E_y^t(x,z) \sim \left(1-\mathcal{R}_{1A}^2\right) \sum_{|m|\leq\frac{d}{(2L_x)}} A_m \sum_{q=0}^{N_q} \mathcal{R}_{1A}^{2q}\tilde{\mathcal{B}}_m^{(q)}(x,z). \tag{9}$$

In (9), the Gabor coefficients A_m are defined in (8), and $\mathcal{R}_{1A}$ is the TM plane-wave Fresnel interface reflection coefficient for incidence from free space at angle θ_A (Fig. 2)

$$\mathcal{R}_{1A} = \frac{\cos\theta_A - \sqrt{\epsilon_{r1}^{(e)} - \sin^2\theta_A}}{\cos\theta_A + \sqrt{\epsilon_{r1}^{(e)} - \sin^2\theta_A}} \tag{10}$$

with $\epsilon_{r1}^{(e)} = \epsilon_{r1} + i\sigma_1/(\omega\epsilon_0)$ denoting the effective relative permittivity of the dielectric layer. Moreover, $\mathcal{T}_{1A} = 1 + \mathcal{R}_{1A}$ and $\mathcal{T}_{2A} = 1 - \mathcal{R}_{1A}$ denote the corresponding interface transmission coefficients from free space to the dielectric and viceversa, respectively; they appear in (9) in the combination $\mathcal{T}_{1A}\mathcal{T}_{2A} = (1-\mathcal{R}_{1A}^2)$. In (9) the q index tags *round-trip* reflections inside the dielectric layer (i.e., 2q *individual* reflections at each layer interface) of the single m-indexed aperture-radiated basis beam (see Fig. 2), with N_q denoting the total number of roundtrips retained (the selection of N_q is discussed in Section V-B). Apart from the explicit internal round-trip reflection coefficient factor $\mathcal{R}_{1A}^{2q}$ in (9), the GB propagator $\tilde{\mathcal{B}}_m^{(q)}$ represents the wavefield contribution at the observer, due to a single m-indexed aperture-radiated basis beam, after undergoing q internal round-trip reflections. The only difference between the present asymptotic

implementation and that in [1, Sec. II-B] is the modeling here of the emerging beam as a *complex ray* emanating from an analytically continued complex virtual focus (see Fig. 2), instead of using the complex off-axis phase correction noted above. This yields the following expression for the CSP GB propagator [formally similar to that in (1.12)]

$$\tilde{\mathcal{B}}_m^q(x,z) \sim -i2^{\frac{5}{4}}(z-\tilde{z}_{fq})\sqrt{\frac{k_0 L_x}{8\pi \tilde{R}_{fmq}^3}} \times \exp\left[i\left(k_0\tilde{\psi}_{mq}+\frac{\pi}{4}\right)\right] \tag{11}$$

where

$$\tilde{\psi}_{mq} = \tilde{R}_{fmq} + x_m \sin\theta_A + \frac{(1+2q)\left(\epsilon_{r1}^{(e)}\cos^2\theta_t - \cos^2\theta_A\right)d_1}{\sqrt{\epsilon_{r1}^{(e)}}\cos^3\theta t} + ib \tag{12}$$

with θ_t denoting the *real* refraction angle for incidence from free space, which is related to θ_A via Snell's law, $\sqrt{\epsilon_{r1}}\sin\theta_t = \sin\theta_A$, wherein (in view of the "slight loss" assumption) the effective (complex) relative permittivity $\epsilon_{r1}^{(e)}$ has been approximated by the real permittivity ϵ_{r1} (i.e., $\sigma_1 = 0$). Moreover, in (11), $\tilde{R}_{fmq}$ represents the *complex distance*

$$\tilde{R}_{fmq} = \sqrt{(x-\tilde{x}_{fmq})^2 + (z-\tilde{z}_{fq})^2}, \mathrm{Re}(\tilde{R}_{fmq}) \geq 0 \tag{13}$$

between the observation point at (x,z) and the *complex virtual focus* $\tilde{\mathbf{r}}_{fmq} \equiv (\tilde{x}_{fmq}, \tilde{z}_{fq})$

$$\tilde{x}_{fmq} = x_m + \frac{(1+2q)\left(\sqrt{\epsilon_{r1}^{(e)}}\sin\theta_t\cos^2\theta_t - \sin\theta_A\cos^2\theta_A\right)d_1}{\sqrt{\epsilon_{r1}^{(e)}}\cos^3\theta_t} + ib\sin\theta_A \tag{14}$$

$$\tilde{z}_{fq} = d_1 - \frac{(1+2q)d_1\cos^3\theta_A}{\sqrt{\epsilon_{r1}^{(e)}}\cos^3\theta_t} + ib\cos\theta_A. \tag{15}$$

In (11)–(15) b is the GB complex displacement parameter (Fresnel length) [cf. (2.22)]

$$b = \frac{(L_x\cos\theta_A)^2}{\lambda_0}. \tag{16}$$

The complex focus coordinates in (14) and (15) are obtained by analytic continuation (to the CSP $\tilde{\mathbf{r}}'_m \equiv (x_m + ib\sin\theta_A, ib\cos\theta_A)$) of the real source point $\mathbf{r}'_m \equiv (x_m, 0)$ in the standard ray optical formulas [17, p. 169] for line-source excitation. Referring to Fig. 2, this corresponds to tracing a ray along a *complex* trajectory (white arrow) from the CSP at $\tilde{\mathbf{r}}'_m$ to the intersection of the *real* beam axis with the *real* layer (lower) interface; from there, the path into the layer proceeds entirely in *real* configuration space, along the beam axis, undergoing q round-trip reflections between the layer boundaries (black arrows). The last segment, which reaches the observer, proceeds in *complex* space, as a *complex ray* (white arrows) emanating from the complex virtual focus $\tilde{\mathbf{r}}_{fmq} = (\tilde{x}_{fmq}, \tilde{z}_{fq})$ in (14) and (15). In real configuration space, these complex rays describe NW paraxial GBs. The layer-transmitted field, due to the single incident basis beam, is obtained by iteration; i.e., summing over the various multiple internal round-trip reflection contributions, weighted by the appropriate reflection/transmission coefficients, as schematized in Fig. 2. Numerically, the above asymptotic procedure was found to be essentially equivalent to the alternative procedure in [1, Sec. II-B] [cf. (1.19a), (1.23)-(1.25)] described earlier, with the same validity constraints to the paraxial far zone of each GB. However, the FD NW-GB synthesis in (9)–(15) was found to be more suitable for analytic inversion to the TD since the CSP-GB propagators $\tilde{\mathcal{B}}_m^{(q)}$ in (11) are formally identical with the infinite space CSP-GB propagators $\tilde{\mathcal{B}}_m$ in (2.20), for which an effective analytic TD inversion technique is already available [2].

The quasireal ray tracing algorithm does *not* account for evanescent contributions arising from surface waves trapped inside the layer. In view of the finite (but electrically large) spatial extent of the tapered aperture field distribution in (1), and the resulting spectrally narrow incident illumination, these wave species can be neglected in the transmitted field. Possible effects when these conditions are *not* satisfied are considered in Section V-C.

IV. Time Domain (TD) Formulation

A. Preliminary Considerations

We note first that an *exact* representation for the field $e_y^t(x,z,t)$ transmitted into the halfspace $z > z_L + d_1$ can be obtained by Fourier inversion (via (4)) of the FD plane-wave synthesis [1], [18, Sec. 14.1]. The (numerically computed) results from this plane-wave synthesis will be used as a reference solution to validate and calibrate the proposed PB syntheses (Section V-A). Next, since the FD CSP GB propagators in (11) are identical with those in (2.20), extension to the time domain (TD) for pulsed excitation can be implemented by following the procedure in [2, Sec. III-A]. In view of the assumed slight Ohmic dispersion in the dielectric layer over the effective bandwidth Ω of the pulse $p(t)$, we apply the previously noted *nondispersive* approximation [12, Sec. IV-A] to the wavenumber in the dielectric layer. We also approximate the frequency-dependent reflection coefficient in (10) by its real, frequency-independent value at $\sigma = 0$, denoted by $\bar{\mathcal{R}}_{1A}$ [cf. (12.37)]. Furthermore, the Gabor lattice parameter L_x is chosen to be frequency independent (see the discussion in [2, Sec. III-A]). Accordingly, anticipating Fourier inversion, the FD Gabor coefficients in (8) are rearranged as

$$A_m = a_m P(\omega)\exp(i\omega t_m), \quad t_m = \frac{\phi_{NL}(x_m)}{c_0} \tag{17}$$

where ϕ_{NL} is defined in (3), and the TD Gabor coefficients

$$a_m = \left(\frac{L_x}{\sqrt{2}}\right)^{\frac{1}{2}} g(x_m) \tag{18}$$

are *real* and *frequency independent*. The FD total field NW-GB synthesis in (9) can thus be rewritten as

$$E_y^t(x,z,\omega) \sim \left(1-\bar{\mathcal{R}}_{1A}^2\right) \sum_{|m|\le\left(\frac{d}{2L_x}\right)} a_m P(\omega)\exp(i\omega t_m) \times \sum_{q=0}^{N_q} \bar{\mathcal{R}}_{1A}^{2q}\tilde{\mathcal{B}}_m^{(q)}(x,z,\omega) \tag{19}$$

with the ω-dependence now shown explicitly.

B. Narrow-Waisted Pulsed Beam (NW-PB) Synthesis of Layer-Transmitted Field

As previously [(2.31) and (2.32)], in order to accommodate the evanescent spectra in the CSP GB propagators $\tilde{\mathcal{B}}_m^{(q)}$, we use the analytic signal representation [14] via the one-sided Fourier transform in (5). As in [2], we first approximate the complex distance $\tilde{R}_{fmq}$ in (13) and the complex coordinates ($\tilde{x}_{fmq}$, $\tilde{z}_{fq}$) in (14) and (15), which are frequency dependent via (16). Specifically, assuming L_x/λ_0 (and therefore b) sufficiently small in the amplitude factor of (11), we approximate the *complex* coordinates ($\tilde{x}_{fmq}$, $\tilde{z}_{fq}$) and the *complex* distance $\tilde{R}_{fmq}$ by the *real* and *frequency-independent* values (x_{fmq}, z_{fq}) and R_{fmq}, obtained by setting $b=0$ and (in view of the "slight loss" assumption) replacing $\epsilon_{r1}^{(e)}$ with ϵ_{r1} [cf. (2.39)]. In the phase factor of (11), given in (12), we use a perturbation expansion about $b=0$ [cf. (12.51)]

$$\tilde{R}_{fmq}(\omega) \approx R_{fmq} - ib\frac{z_{bmq}}{R_{fmq}} = R_{fmq} - i\omega\frac{z_{bmq}(L_x\cos\theta_A)^2}{2\pi c_0 R_{fmq}} \tag{20}$$

with $z_{bmq} = \sin\theta_A(x-x_{fmq}) + \cos\theta_A(z-z_{fq})$ denoting the axial beam coordinate (Fig. 2). The range of validity of the approximation in (20) is discussed in Section IV-C. As shown in Section V-B, this approximation has been found to outperform the paraxial approximation used in [2] [cf. (2.40)].

As in [2], we use a class of Rayleigh (differentiated Gaussian) pulses [cf. (2.37)]

$$p(t) = P_0\frac{d^j}{dt^j}\exp\left[-\left(\frac{t-\frac{T}{2}}{\varsigma T}\right)^2\right] \tag{21}$$

where P_0 is a normalization constant, and the variance ς is chosen so that the pulse width of $p(t)$ is $\sim T$. For these pulses, and with the approximations discussed above, the analytic Fourier inversion of the FD NW-PB synthesis in (19) can be performed in closed form (see [2], [12] for details), yielding the following NW-PB synthesis [cf. (2.33)]

$$e_y^t(x,z,t) \sim (1-\bar{\mathcal{R}}_{1A}^2) \sum_{|m|\le\left(\frac{d}{2L_x}\right)} a_m \sum_{q=0}^{Nq} \bar{\mathcal{R}}_{1A}^{2q}\mathrm{b}_m^{(q)}(x,z,t-t_m) \tag{22}$$

with t_m and a_m being defined in (17) and (18), respectively, and with the NW-PB propagator $\mathrm{b}_m^{(q)}$ given by (generalizing (2.44) as shown in [12, Sec. IV-C])

$$\begin{aligned}\mathrm{b}_m^{(q)}(x,z,t) &= \mathrm{Re}\Bigg\{(-i)^j\beta_{mq}\Bigg[\mathcal{T}_{mq}\Gamma\left(\frac{3+2j}{4}\right)\mathrm{M}_1^{(j)}\left(\frac{t-\tau_{mq}-\frac{T}{2}}{\mathcal{T}_{mq}}\right) \\ &\quad -2i\left(t-\tau_{mq}-\frac{T}{2}\right)\Gamma\left(\frac{5+2j}{4}\right) \\ &\quad \times\mathrm{M}_2^{(j)}\left(\frac{t-\tau_{mq}-\frac{T}{2}}{\mathcal{T}_{mq}}\right)\Bigg]\Bigg\}.\end{aligned} \tag{23}$$

In (23), $\beta_{mq} = 2^{j+1/2}\pi^{-1/2}(\mathcal{T}_{mq})^{-j-5/2}\Lambda_{mq}P_0\varsigma T$, $\mathcal{T}_{mq} = \sqrt{T_{mq}^2+\varsigma^2T^2}$, and

$$\Lambda_{mq} = i2^{\frac{5}{4}}\sqrt{\frac{L_x}{8\pi c_0 R_{fmq}^3}}(z-z_{fq})\exp\left(-\kappa_1 R_{Lq}+\frac{i\pi}{4}\right) \tag{24}$$

$$\kappa_1 = \frac{\sigma_1}{2c_0\epsilon_0\sqrt{\epsilon_{r1}}}, \quad R_{Lq} = (1+2q)\frac{d_1}{\cos\theta_t} \tag{25}$$

$$\begin{aligned}\tau_{mq} &= c_0^{-1}\Bigg[R_{fmq} + x_m\sin\theta_A \\ &\quad +\frac{(1+2q)(\epsilon_{r1}\cos^2\theta_t-\cos^2\theta_A)d_1}{\sqrt{\epsilon_{r1}}\cos^3\theta_t}\Bigg]\end{aligned} \tag{26}$$

$$T_{mq} = c_0^{-1}L_x\cos\theta_A\sqrt{\frac{2}{\pi}\left(1-\frac{z_{bmq}}{R_{fmq}}\right)}. \tag{27}$$

Moreover, $\Gamma(\cdot)$ is the gamma function [19], and

$$\begin{aligned}\mathrm{M}_1^{(j)}(t) &= {}_1\mathrm{F}_1\left(\frac{3+2j}{4},\frac{1}{2},-t^2\right) \\ \mathrm{M}_2^{(j)}(t) &= {}_1\mathrm{F}_1\left(\frac{5+2j}{4},\frac{3}{2},-t^2\right)\end{aligned} \tag{28}$$

with ${}_1\mathrm{F}_1(u,v,t)$ denoting the Kummer confluent hypergeometric function [19]. The functions $\mathrm{M}_{1,2}^{(j)}$ can be computed efficiently using the rapidly converging expansions in [12, App. B].

C. Assessment of Accuracy: Nondimensional (ND) Estimators

In [2, Sec. III-C], the constraints arising from the sequence of approximations utilized to obtain explicit closed form expressions for the PB propagator analogous to (23) have been formalized in terms of a nondimensional (ND) estimator which embodies the important (suitably scaled) problem parameters. This ND estimator was found to be useful for calibration of the algorithm and systematic estimation of its range of applicability. We adopt a similar format here, based on the approximations discussed in Section IV-A. The most stringent overall constraint is related to the perturbation expansion in b in (20), which also determines the maximum allowable lattice period L_x via (16) and thereby the minimum number of beams via $N_b = d/L_x$ [see (22)], for specified pulsed bandwidth Ω, linear phasing θ_A, and observation point (x, z). This constraint can be formalized

by enforcing the *smallness* of the $\mathcal{O}(b^2)$ term neglected in (20), i.e., $|\mathcal{O}(b^2)/\mathcal{O}(b)| \ll 1$

$$\left|\frac{\partial_b^2 \tilde{R}_{fmq}|_{b=0}}{z_{bmq}}\right| bR_{fmq} \ll 1, \quad \partial_b^2 \equiv \frac{\partial^2}{\partial b^2}. \tag{29}$$

It is expedient to rewrite the complex distance $\tilde{R}_{fmq}$ in terms of the beam coordinates (x_{bmq}, z_{bmq}) in Fig. 2

$$\tilde{R}_{fmq} = \sqrt{x_{bmq}^2 + (z_{bmq} - ib)^2}, \quad \mathrm{Re}(\tilde{R}_{fmq}) \geq 0 \tag{30}$$

with $x_{bmq} = \cos\theta_A(x - x_{fmq}) - \sin\theta_A(z - z_{fq})$, and z_{bmq} already defined after (20). From (30), one obtains $\partial_b^2 \tilde{R}_{fmq}|_{b=0} = -x_{bmq}^2/R_{fmq}^3$, and therefore the constraint in (29) becomes

$$\frac{x_{bmq}^2 b}{R_{fmq}^2 z_{bmq}} \ll 1. \tag{31}$$

Using the bounds $|x_{bmq}| < R_{fmq}$ [see (30)] and $z_{bmq} = (z - z_{fq})/\cos\theta_A > (z - d_1)/\cos\theta_A$, the constraint in (31) may be replaced by

$$\frac{b\cos\theta_A}{z - d_1} \ll 1 \tag{32}$$

which is independent of the individual beam and multiple reflection indexes m and q, respectively, and is formally identical with that in [2] [cf. (2.43)]. Therefore, as in (2.59), we obtain the ND estimator

$$Q \equiv N_b^{-1}\sqrt{\frac{\kappa(\cos\theta_A)^3}{\chi}} \ll 1. \tag{33}$$

Here, the integer $N_b = d/L_x$ represents the number of beams in the expansion (22), $\kappa = \Omega T/2\pi$ is the normalized bandwidth of the pulse $p(t)$, and $\chi = (z - d_1)/F_d$ is the distance to the observation plane, reduced by the layer thickness d_1 and scaled by the Fresnel distance of the aperture, $F_d = d^2/(c_0 T)$. The ND estimator $Q \ll 1$ repackages the constraint in (32) in terms of a combination of useful physical problem parameters, through which the change in one can be compensated by a change in the others within the constraint. For example, at *larger* observation distances z, *fewer* beams are required. However, Q in (33) does not contain the number of retained internal round-trip reflections N_q, nor the "slight loss" assumption in Section IV-A. Therefore, it gives no information about the associated compensation mechanisms within the overall constraints. These issues are dealt with separately in Section V.

V. Numerical Results

A. Reference Solution and Simulation Parameters

As noted earlier, the TD transmitted field reference solution used to validate and calibrate the PB synthesis is based on Fourier inversion of the exact FD spectral integral representation in [1], [18, Sec. 14.1]; the FD solution has been implemented via brute-force numerical quadrature (five-point Gaussian [20], 20 points per spectral period) at 100 different frequencies within the pulse bandwidth. Here, the *exact* effective permittivity $\epsilon_{r1}^{(e)}$ is used for the dielectric layer medium.

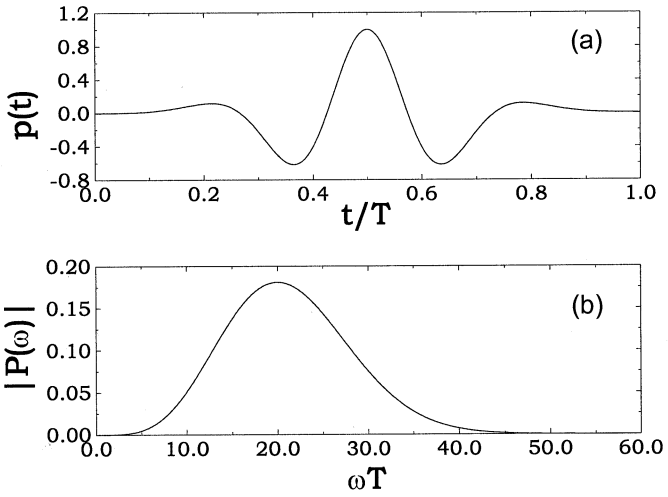

Fig. 3. Fourth-order Rayleigh pulse ($j = 4$, $P_0 = T^4/30\,000$, $\varsigma = 1/\sqrt{50}$). (a) Temporal profile in (21). (b) Spectrum (magnitude).

The resulting frequency samples are smoothed through local Padé-approximation [20] and filtered by the pulse spectrum $P(\omega)$. The desired TD solution is then obtained via standard inverse (1024-point) fast Fourier transform routines [20].

Extensive numerical simulations have been performed in order to validate and calibrate the PB syntheses in Section IV-B against the reference solution. Representative results are presented below. Since the field transmitted into the halfspace $z > z_L + d_1$ does not depend on the layer location z_L between the aperture and observation planes, we have assumed $z_L = 0$ in all simulations. The temporal excitation is the wideband Rayleigh pulse shown in Fig. 3, obtained from (21) with $j = 4$, $P_0 = T^4/30\,000$, and $\varsigma = 1/\sqrt{50}$. A pulse-bandwidth value $\Omega T = 40$ is assumed throughout (see Fig. 3), which sets the reference level for the ND estimator Q in (33). In the numerical results of Figs. 4–6 we have normalized all length coordinates with respect to the aperture width d, which has been chosen for convenience as $d = 1$.

B. Focusing Aperture Field Distributions

From an extensive series of simulations for different ranges of problem parameters, we have selected for presentation a particularly challenging example: excitation by a Gaussian-tapered aperture field distribution with linear and quadratic delay

$$g(x) = \exp\left(\frac{-\alpha x^2}{d^2}\right), \quad \phi(x) = x\sin\theta_A - \beta x^2 \tag{34}$$

which generates a wide Gaussian-tapered wavepacket, with the parameter α in (34) chosen such that the initial distribution tends to zero for $|x| > d/2$. Depending on the sign of β, the radiated wavepacket can either be *focusing* ($\beta > 0$) or *defocusing* ($\beta < 0$). As noted above, we consider the nontrivial focusing case, which encompasses caustic-generating wave phenomena that cannot be analyzed via standard nonuniform ray asymptotics due to its failure in caustic region transitions. Transition of this nonstandard focusing PB wavepacket through the layer in the near zone of the aperture poses an overall wave problem of substantial complexity. We assume a rather large (in terms of the

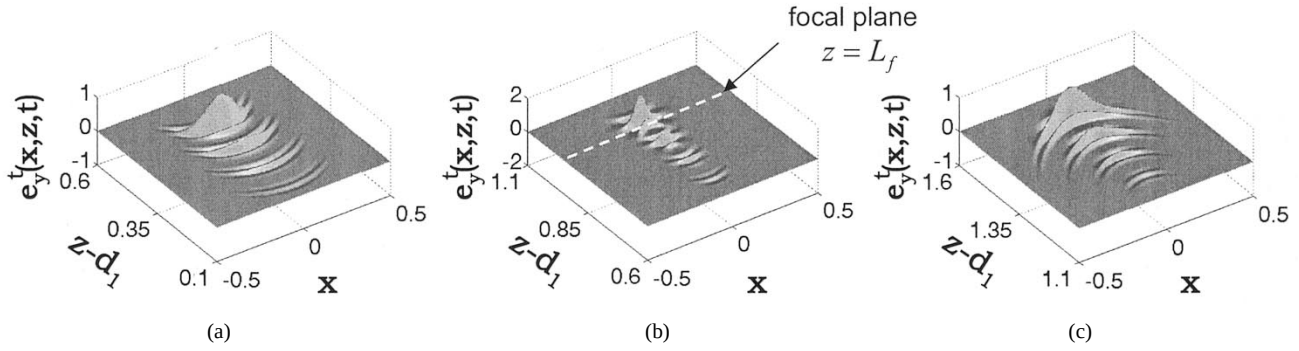

Fig. 4. Geometry as in Fig. 1, with $d = 1$ (arbitrary units), $c_0T = 0.1d$, $z_L = 0$, $\epsilon_{r1} = 10$, $\sigma_1 = 0.01$ S/m, $d_1 = 0.5c_1T$. Gaussian-tapered quadratic delay aperture field distribution in (34), with $\alpha = 20$, $\theta_A = 0$, and $\beta = 0.5$ (focal plane at $L_f = d_1 + 1$, i.e., $\chi = 0.1$). Instantaneous snapshots of the transmitted field at various times, computed via the reference solution.: (a) $c_0t = 0.55(z < L_f)$, (b) $c_0t = 1.08$ (focusing region, $z - d_1 \approx L_f - d_1 = 1$; note different amplitude scale), and (c) $c_0t = 1.6(z > L_f)$.

pulse width T) aperture ($d = 10c_0T$), and a slightly lossy dielectric layer ($\epsilon_{r1} = 10, \sigma_1 = 0.01$ S/m), which has a thickness $d_1 = 0.5c_1T$ chosen so as to allow time resolution of the various multiples; $c_1 = c_0/\sqrt{\epsilon_{r1}}$ denotes the wavespeed in the dielectric layer. Under these conditions, the short-pulse asymptotic and the "slight loss" assumptions in our algorithm should be well within the range of validity, leading us to expect good accuracy with a moderate number of beams (N_b) and retained internal round-trip reflections (N_q). We show here only the case $\theta_A = 0$ (normal incidence), for which the distance L_f from the aperture to the location of substantial focusing of the layer-transmitted field is taken to be $L_f = d_1 + 1/(2\beta)$ (see Fig. 1 with $z_L = 0$), which will subsequently be referred to as the "focal plane" (for $\theta_A \neq 0$, see the performance estimates in Table I). In our simulations, numerical values have been adjusted to produce focusing in the near zone of the aperture ($L_f = d_1 + 1$, i.e., $\chi = 0.1$ in (33); note the previously mentioned normalization to $d = 1$). A sequence of instantaneous snapshots of the radiated field at different times, computed via the reference solution in Section V-A, is shown in Fig. 4. One observes that the broad space-time wavepacket, starting from the initial distribution in (2) [with (34)], exhibits a concave (focusing) wavefront on its way to the focal plane, i.e., for $z < L_f$ [Fig. 4(a)]; its maximum spatial localization occurs at the focal plane $z = L_f$ [Fig. 4(b)], with expansion (convex wavefront) beyond the focal plane [Fig. 4(c)]. These effects resemble those already observed in the absence of the layer (cf. [2]), the only difference now being the presence of several wavepackets arising from multiple reflections inside the layer (see Fig. 2). For this example, the accuracy of the PB syntheses is illustrated in Fig. 5. Specifically, Fig. 5(a) shows the comparison (with excellent agreement) between the PB synthesis and the reference solution at a fixed observation point on the focal plane; due to focusing, the amplitude of the wavefield is about 50% stronger than the pulse profile maximum in Fig. 3(a) (note the pulse distortion due to the focal plane transition). In these and all other examples, the number of retained internal round-trip reflections has been arrived at by using the criterion suggested in [1], i.e., truncating the q-summation in (22) when the magnitude of the first omitted term is less than 0.1% of that of the leading term. The number of NW basis PBs in the expansion in (22) is arrived at using the pragmatic *scrambling* criterion in [2], [12], i.e., insensitivity of the result with respect to different combinations of the beam/lattice

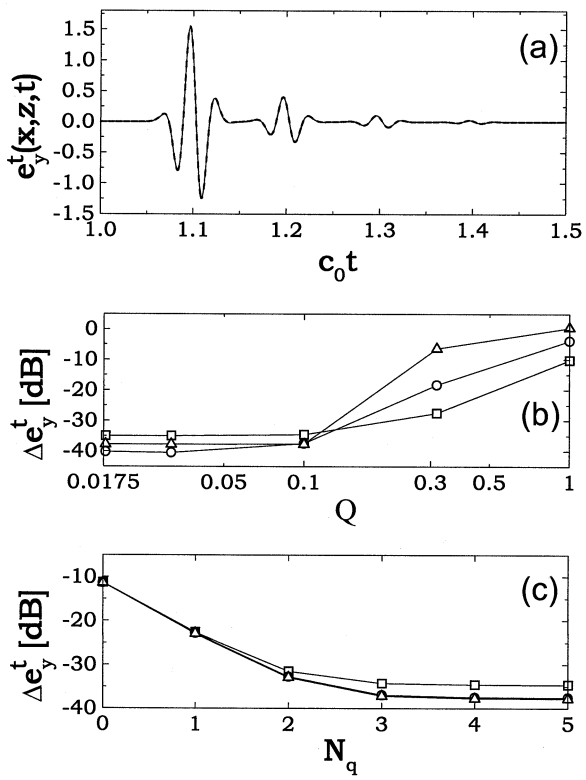

Fig. 5. Parameters as in Fig. 4. (a) Comparison between PB synthesis and reference solution for transmitted field at a fixed observation point on the focal plane ($x = 0$, $z = d_1 + 1$, i.e., $\chi = 0.1$). ——Reference solution; - - - PB synthesis with $N_b = d/L_x = 80$ beams ($Q = 0.1$) and $N_q = 3$ internal round-trip reflections. Reference solution and PB synthesis coincide on the scale of the plot. (b) and (c) rms error versus Q (at $N_q = 3$) and versus N_q (at $Q = 0.1$), respectively, for $x = 0$ and various observation distances. —□—$z = d_1 + 0.25(\chi = 0.025)$; —○—$z = d_1 + 2(\chi = 0.2)$; —△—$z = d_1 + 10(\chi = 1)$.

configuration parameters; the corresponding value of the ND estimator in (33) is $Q \approx 0.1$.

To better quantify the convergence of the NW-PB synthesis and the role of the ND estimator Q in (33), we have introduced the normalized rms (energy) error

$$\Delta e_y^t = \frac{\int_{-\infty}^{\infty} \left| e_y^t(x,z,t) - e_{yr}^t(x,z,t) \right|^2 dt}{\left[\int_{-\infty}^{\infty} \left| e_y^t(x,z,t) \right|^2 dt \int_{-\infty}^{\infty} \left| e_{yr}^t(x,z,t) \right|^2 dt \right]^{\frac{1}{2}}} \quad (35)$$

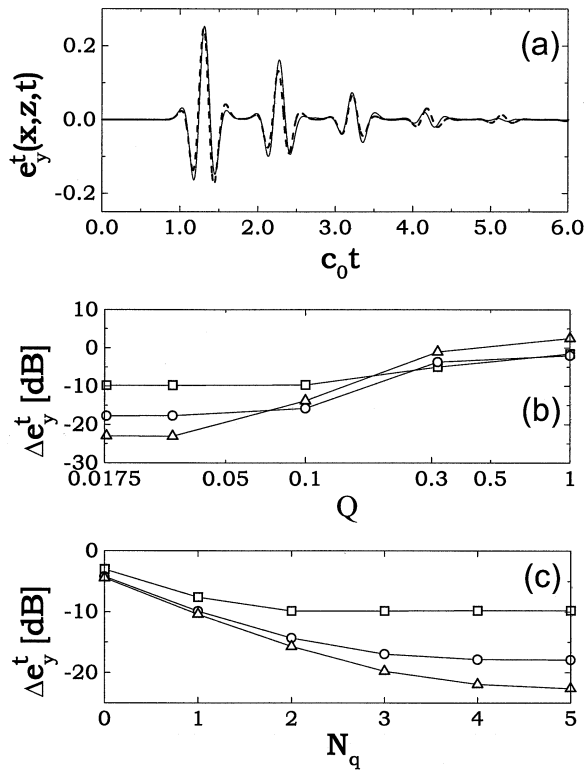

Fig. 6. Parameters as in Fig. 4, but with a cosine-tapered linearly-phased ($\theta_A = 70°$) aperture field distribution, and a longer pulse ($c_0T = d$). (a) Comparison between PB synthesis and reference solution for transmitted field at a fixed observation point on the beam axis θ_A ($x = 0.32$, $z = d_1 + 0.1$, i.e., $\chi = 0.1$). ——Reference solution; - - - PB synthesis with $N_b = d/L_x = 52$ beams ($Q = 0.03$) and $N_q = 4$ internal round-trip reflections. (b), (c) rms error versus Q (at $N_q = 4$) and versus N_q (at $Q = 0.03$), respectively, for various observation points on the beam axis. —□—$x = 0.32$, $z = d_1 + 0.1(\chi = 0.1)$; —○—$x = 1.42$, $z = d_1 + 0.5(\chi = 0.5)$; —△—$x = 2.8$, $z = d_1 + 1(\chi = 1)$.

with e_{yr}^t denoting the reference solution. The convergence with respect to the ND estimator Q is illustrated in Fig. 5(b), for observation points *before*, *at*, and *beyond* the focal plane; each curve refers to a fixed observation point, and is parameterized in terms of Q by varying the remaining free parameter $N_b = d/L_x$ (the number of beams) in (33). In accord with (33), the rms error decreases monotonically with decreasing Q (i.e., increasing N_b), with *weak* dependence on the observation distance z. Quantitatively, values of $Q \approx 0.1$ [as in Fig. 5(a)] yield rms errors < -30 dB; this threshold value is consistent with those obtained in [2, Sec. IV-D] in connection with free-space radiation. The convergence with respect to the number N_q of multiple internal round-trip reflections retained in the PB synthesis is plotted as rms error versus N_q in Fig. 5(c). For these examples it is observed that $N_q = 2$ suffices to yield rms errors < -30 dB. However, depending on the properties of the layer and on the aperture phasing, one may require a larger number of internal round-trip reflections. It is interesting to note that, unlike what was observed in the free-space case [2], [11], the convergence on the focal plane turns out to be not particularly critical (compare Fig. 5(b) with [11, Fig. 13]). We verified that this difference stems from use of the perturbation expansion in (29), instead of the paraxial approximation utilized in [2], [11]. While for linear delay/phasing, the two approximations are found to perform almost identically, for quadratic-delay distributions, the perturbation expansion in (29) is found to perform better. An extensive series of numerical simulations with various parameter combinations has been carried out for the focusing aperture field distributions in (34), with representative results summarized in Table I. Similar accuracy and convergence behavior have been observed in applications involving *abruptly-truncated* and *multilobe* aperture field distributions [21].

TABLE I
FOCUSING APERTURE FIELD DISTRIBUTION. TYPICAL rms ERRORS FOR VARIOUS COMBINATIONS OF ϵ_{r1}, σ_1, d_1, θ_A, AND β. ALL OTHER PARAMETERS ARE AS IN FIG. 4. THE rms ERRORS ARE BASED ON AVERAGE VALUES FOR A SET OF 9 NUMERICAL EXPERIMENTS AT DIFFERENT OBSERVATION POINTS (WHERE THE FIELD IS SIGNIFICANTLY NONZERO) IN THE NEAR, INTERMEDIATE AND FAR ZONE (INCLUDING THE FOCAL PLANE). THE NUMBER OF BEAMS N_b IN THE EXPANSION IS CHOSEN SUCH THAT $Q \approx 0.1$, WHEREAS THE NUMBER OF INTERNAL ROUNDTRIP REFLECTIONS N_q IS CHOSEN SO AS TO RENDER THE FIRST OMITTED TERM LESS THAN 0.1% OF THE LEADING TERM

ϵ_{r1}	σ_1 [S/m]	$d_1/(c_1T)$	θ_A	β	Δe_y^t [dB]
6	0.03	0.8	30^o	2	-28
2	0.02	1.5	40^o	1	-32
15	0.05	0.5	20^o	2.5	-29
8	0.1	0.1	60^o	0.67	-30
18	0.06	1	10^o	1.25	-33

C. Range of Applicability and Computational Features

In the examples presented so far, geometric configurations and parameters have been chosen so as to satisfy the *intrinsic* model constraints (short-pulse asymptotics, slight loss), with emphasis on the convergence properties quantified by the ND estimator (or, equivalently, the number of beams, N_b) as well as the number of retained internal round-trip reflections, N_q. When the intrinsic model constraints are no longer satisfied, the above convergence criteria become suspect. For example, for a cosine-tapered linear-delay aperture field distribution profile with $g(x) = \cos(\pi x/d)$, $\phi(x) = x \sin\theta_A$, and $c_0T = d$ (i.e., a pulse ten times longer than in the previous example), the radiated field does not exhibit quasiplane-wave character and therefore contains evanescent constituents which may interact with a nearby layer so as to couple to possible surface-wave fields. These evanescent contributions to the layer-transmitted field are not accounted for in our GB syntheses but are accounted for in the reference solution. They are negligible (exponentially decaying) for observation distances sufficiently far from the top surface of the layer, but may become significant when the observation point is close to the layer. This is illustrated in Fig. 6(a) which shows the comparison between the NW-PB synthesis and the reference solution for an observation point close to the layer ($z = d_1 + 0.1$, i.e., $\chi = 0.1$). The PB synthesis still performs quite well ($\Delta e_y^t \approx -10$ dB), but one observes discrepancies with respect to the reference solution which, as shown in Fig. 6(b) and (c), respectively, *cannot* be repaired by decreasing Q (i.e., increasing N_b) or by increasing N_q. However, as the observation distance is progressively increased, the accuracy improves, reaching rms errors on the order of -20 dB in the in-

TABLE II
FOCUSING APERTURE FIELD DISTRIBUTION. CALIBRATED RANGE OF APPLICABILITY OF OUR ALGORITHM

Parameter	Calibrated range
d	$> 5c_0T$
θ_A	$< 75^o$
β	< 5
d_1	$> 0.05c_1T$ $< 5c_1T$
ϵ_{r1}	< 25
σ_1	$< 0.05\Omega\epsilon_0\epsilon_{r1}$
χ	> 0.02

termediate and far zone. We can speculate that the near-zone poorer accuracy stems from the neglected evanescent contributions, but confirmation would require more sophisticated propagation models than those in Section IV-B.

The calibrated range of applicability of the algorithm, obtained through several hundred numerical simulations involving various aperture field distributions and different combinations of problem parameters, is summarized in Table II. In this range, reasonably accurate predictions ($\Delta e_y^t \lesssim -20$ dB on average) should be expected. Parameter combinations falling outside this range need not to be doomed to failure a priori, but they must be calibrated independently.

Concerning the computational features of the algorithm, typical computing times, for an *entire* 1000-sample waveform on a 700 MHz PC, range from 0.06 secs. (for $N_b = 10$, $N_q = 2$) to 8.2 s (for $N_b = 500$, $N_q = 10$), with very modest memory requirements (about 10 kbytes on average). For the same problem, typical computing times for our reference solution (with simulation parameters as in Section V-A) are on the order of 2 min on average.

VI. CONCLUSION

A Gabor-based narrow-waisted quasiray Gaussian beam algorithm, which extends to the TD a previously developed FD algorithm [1], has been presented for short-pulse 2-D wavefields radiated by 1-D aperture field distributions and propagated through a planar slightly lossy dielectric layer. Accuracy assessments have been formalized analytically in terms of critical nondimensional estimators, and calibrated against a numerical independently generated rigorous reference solution for an extensive series of simulations that involve linearly and nonlinearly phased (focusing) pulsed aperture field distributions. The numerical results are encouraging and confirm that the previously established utility of the algorithm in the FD remains intact in the TD. The TD extension of previously developed FD beam algorithms for propagation through *curved* layers [9], [10] is under consideration, as is the extension to multiple layer configurations. We have not yet dealt with extension to *dispersive* dielectric layers, which would involve more sophisticated PB propagation models.

REFERENCES

[1] J. J. Maciel and L. B. Felsen, "Gaussian beam analysis of propagation from an extended aperture distribution through dielectric layers, part I - plane layer," *IEEE Trans. Antennas Propagat.*, vol. 38, pp. 1607–1617, Oct. 1990.

[2] V. Galdi, L. B. Felsen, and D. A. Castañon, "Narrow-waisted Gaussian beam discretization for two-dimensional time-dependent radiation from large apertures," *IEEE Trans. Antennas Propagat.*, vol. 49, pp. 1322–1332, Sept. 2001.

[3] L. B. Felsen and F. Niu, "Spectral analysis and synthesis options for short pulse radiation from a point dipole in a grounded dielectric layer," *IEEE Trans. Antennas Propagat.*, vol. 41, pp. 747–754, June 1993.

[4] F. Niu and L. B. Felsen, "Time-domain leaky modes on layered media: dispersion characteristics and synthesis of pulsed radiation," *IEEE Trans. Antennas Propagat.*, vol. 41, pp. 755–761, June 1993.

[5] ——, "Asymptotic analysis and numerical evaluation of short pulse radiation from a point dipole in a grounded dielectric layer," *IEEE Trans. Antennas Propagat.*, vol. 41, pp. 762–769, June 1993.

[6] R. W. P. King and S. S. Sandler, "The electromagnetic field of a vertical electric dipole in the presence of a three-layered region," *Radio Sci.*, vol. 29, no. 1, pp. 97–113, Jan.–Feb. 1994.

[7] A. G. Tijhuis and A. R. Bretones, "Transient excitation of a layered dielectric medium by a pulsed electric dipole," *IEEE Trans. Antennas Propagat.*, vol. 48, pp. 1673–1684, Oct. 2000.

[8] J. J. Maciel and L. B. Felsen, "Systematic study of fields due to extended apertures by Gaussian beam discretization," *IEEE Trans. Antennas Propagat.*, vol. 37, pp. 884–892, July 1989.

[9] ——, "Gaussian beam analysis of propagation from an extended aperture distribution through dielectric layers, part II—circular cylindrical layer," *IEEE Trans. Antennas Propagat.*, vol. 38, pp. 1618–1624, Oct. 1990.

[10] ——, "Gabor-based narrow-waisted Gaussian beam algorithm for transmission of aperture-excited 3D vector fields through arbitrarily shaped 3D dielectric layers," Radio Sci., vol. 37, no. 6, Nov.–Dec. 2003, to be published.

[11] V. Galdi, L. B. Felsen, and D. A. Castañon, "Time-domain radiation from large two-dimensional apertures via narrow-waisted Gaussian beams," *IEEE Trans. Antennas Propagat.*, vol. 51, pp. 78–88, Jan. 2003.

[12] ——, "Quasiray Gaussian beam algorithm for short-pulse two-dimensional scattering by moderately rough dielectric interfaces," *IEEE Trans. Antennas Propagat.*, vol. 51, pp. 171–183, Feb. 2003.

[13] V. Galdi, L. B. Felsen, and D. A. Castañon, "3-D short pulse scattering by moderately rough dielectric interfaces via quasiray Gaussian beams," in *Proc. 2002 IEEE Antennas Propagat. Int. Symp.*, vol. 4, San Antonio, TX, June 16–21, 2002, pp. 252–255.

[14] T. B. Hansen and A. D. Yaghjian, *Plane-Wave Theory of Time-Domain Fields: Near-Field Scanning Applications*. Piscataway, NJ: IEEE Press, 1999.

[15] W. D. Wang and G. A. Deschamps, "Application of complex ray tracing to scattering problems," *Proc. IEEE*, vol. 62, pp. 7541–7551, Nov. 1974.

[16] X. J. Gao and L. B. Felsen, "Complex ray analysis of beam transmission through two-dimensional radomes," *IEEE Trans. Antennas Propagat.*, vol. 33, pp. 963–975, Sept. 1985.

[17] L. B. Felsen and N. Marcuvitz, *Radiation and Scattering of Waves*. Englewood Cliffs, NJ: Prentice-Hall, 1973.

[18] L. M. Brekhovskikh, *Waves in Layered Media*. New York: Academic, 1980.

[19] M. Abramowitz and I. A. Stegun, *Handbook of Mathematical Functions*. New York: Dover, 1964.

[20] W. H. Press, S. A. Teukolsky, W. T. Vetterling, and B. P. Flannery, *Numerical Recipes in C: The Art of Scientific Computing*, 2nd ed. Cambridge, U.K.: Cambridge Univ. Press, 1992.

[21] V. Galdi and L. B. Felsen, "Two-dimensional narrow-waisted Gaussian beam analysis of pulsed propagation from extended planar one-dimensional aperture field distributions through planar dielectric layers," in *Ultra-Wideband Short Pulse Electromagnetics 6*, E. L. Mokole, Ed. New York: Kluwer/Plenum, 2003.

Vincenzo Galdi (M'98) was born in Salerno, Italy, on July 28, 1970. He received the Laurea degree (*summa cum laude*) in electrical engineering and the Ph.D. degree in applied electromagnetics from the University of Salerno, Italy, in 1995 and 1999, respectively.

From Apri1 to December 1997, he held a visiting position in the Radio Frequency Division, European Space Research and Technology Centre (ESTEC-ESA), Noordwijk, The Netherlands. From September 1999 to August 2002, he held a Research Associate position in the Department of Electrical and Computer Engineering, Boston University, Boston, MA. In September 2002, he was appointed Associate Professor of Electromagnetics, and joined the Department of Engineering, University of Sannio, Benevento, Italy, where he is currently working. His research interests include analytical and numerica1 techniques for wave propagation in complex environments, electromagnetic chaos, and inverse scattering.

Dr. Galdi received the 2001 International Union of Radio Science (URSI) "Young Scientist Award." He is a Member of Sigma Xi.

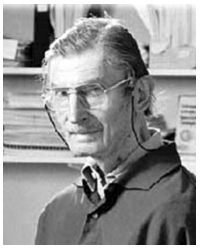

Leopold B. Felsen (S'47–M'54–SM'55–F'62–LF'90) was born in Munich, Germany, on May 7, 1924. He received the B.E.E., M.E.E, and D.E.E. degrees from the Polytechnic Institute of Brooklyn, Brooklyn, NY, in 1948, 1950, and 1952, respectively.

He emigrated to the United States in 1939 and served in the U.S. Army from 1943 to 1946. After 1952, he remained with the Polytechnic (now Polytechnic University), gaining the position of University Professor in 1978. From 1974 to 1978, he was Dean of Engineering. In 1994, he resigned from the full-time Polytechnic faculty and was granted the status of University Professor Emeritus. He is now Professor of Aerospace and Mechanical Engineering and Professor of Electrical and Computer Engineering at Boston University, Boston, MA (part-time). He is the author or coauthor of over 350 papers and of severa1 books, including the classic *Radiation and Scattering of Waves* (Piscataway, NJ: IEEE Press, 1994). He is an Associate Editor of severa1 professional journals and an Editor of the *Wave Phenomena Series* (New York: Springer-Verlag). His research interests encompass wave propagation and diffraction in complex environments and in various disciplines, high-frequency asymptotic and short-pulse techniques, and phase-space methods with an emphasis on wave-oriented data processing and imaging.

Dr. Felsen received the the Guggenheim Fellowship in 1973, the Humboldt Foundation Senior Scientist Award in 1981, the IEEE/APS best paper award for 1969, and was coauthor for 1974, 1981, the R. W. P. King Award for 1984, 1986, and 2000, the Balthasar van der Pol Gold Medal from the International Union of Radio Science (URSI) in 1975, an honorary doctorate from the Technical University of Denmark in 1979, an IEEE Centennial Medal in 1984, the IEEE Heinrich Hertz Gold Medal for 1991, the APS Distinguished Achievement Award for 1998, the IEEE Third Millenium Medal in 2000 (nomination by APS), the IEEE Electromagnetics Award for 2003, and three Distinguished Faculty Alumnus Awards from Polytechnic University. In 1974 he was an IEEE/APS (Antennas and Propagation Society) Distinguished Lecturer. In 1977, he was elected to the National Academy of Engineering. He is a Member of Sigma Xi and a Fellow of the Optical Society of America and the Acoustical Society of America. He has held named Visiting Professorships and Fellowships at universities in the United States and aboard, including His Poet's Corner appears sporadically in the IEEE/APS Magazine. He has served on the APS Administrative Committee from 1963–1966, and was Vice Chairman and Chairman for both the United States (1966–1973) and the International (1978–1984) URSI Commission B.